Journal of Physics: Conference Series **659** (2015) 012011 doi:10.1088/1742-6596/659/1/012011

Robot Kinematics Identification: KUKA LWR4+ Redundant Manipulator Example

Sergey Kolyubin, Leonid Paramonov, and Anton Shiriaev

Dept. of Engineering Cybernetics, Norwegian University of Science and Technology, NO-7491, Trondheim, NORWAY

E-mail: {sergey.kolyubin, leonid.paramonov, anton.shiriaev}@ntnu.no

Abstract. This work is aimed at a comprehensive discussion of algorithms for the kinematic parameters identification of robotic manipulators. We deal with an open-loop geometric calibration task, when a full 6D robot's end-effector pose is measured. Effective solutions of such a task is of high interest in many practical applications, because it can dramatically improve key robot characteristics. On the first step, we select optimal calibration configurations. A comparative analysis of three different algorithms and two observability indexes used for numerical optimization is provided. Afterwards, using the acquired and pre-processed experimental data we identify modified Denavit-Hartenberg parameters of the manipulator. Estimates are obtained resolving original nonlinear forward kinematics relations. Finally, we compare nominal and calibrated geometric parameters and show how much deviations in these parameters affect robot positioning accuracy. To the best of our knowledge, such integrated efforts are new for the KUKA LWR4+ robot and Nikon K610 optical coordinate measuring machine (CMM), which were used in the study. Discussion of practical issues on how to organise the experiment is an additional contribution of this work. The proposed procedure is highly automated and can be implemented to improve manipulator's performance on a periodic basis.

1. Introduction

Absolute accuracy of a robot's tool positioning is one of its key performance characteristics that has a dedicated test standard [1]. It matters for almost all applications of industrial manipulators, but precise positioning is even more important for such tasks as laser welding, riveting, or automated fibre placement in composite manufacturing as well as for contact operations like grinding or drilling.

This is an example, where an effective parameters identification technique finds a good application, and competence areas of control and robotics communities perfectly complement each other.

While the industrial manipulators mechanics and manufacturing techniques are constantly improving, there is still a crucial trade-off between price and quality, therefore manufacturing and assembly defects still exist and cause significant deviation of the real robot parameters from its nominal values specified on the design phase. Such offsets in parameters used by a motion planner or a motion controller can significantly degrade the overall system performance and even cause the equipment damage. A way to handle the problem and improve the robot accuracy just on a software level without changing the mechanical structure of a robot is the proper calibration.

Some of the industrial robots' manufactures now offer an option, when a manipulator comes with pre-calibrated parameters. However, there is a need for an identification procedure that can be implemented on-site on a periodic basis in case if a robot was relocated, and simply because parameters can drift with time.

The calibration problem was extensively developed in fundamental works of Hollerbach, Khalil, Born and Menq, Daney, and others, and still remains an active research area [10, 11].

There are sources of robot positioning errors of different nature such as joint's and link's flexibility or gear backlash and friction, but according to [12], poor estimation of basic parameters defining robot geometry could be responsible for up to 90% of these errors. Here we discuss an *open-loop geometric calibration* meaning that we estimate robot's geometric parameters from experiments when the robot end-effector is not physically fixed in space, but its position is defined by an external measurement device.

The calibration procedure should be properly organized. Indeed, from the very beginning an engineer is required to choose a number of robot's configurations (poses) that will be most informative and insensitive to noise in further processing of measurement records. Such poses are typically found numerically via optimizing one or several aggregated criteria describing sensitivity of parameters used in solution of a forwards kinematics for a robot. Moreover, this preparatory step if often used to define sets of identifiable and non- or poorly identifiable parameters. These sets depend on the arm kinematics and setup in particular, and can be analysed in advance by detecting linear dependent columns of the parametric Jacobian for a random set of configurations [9]. In this paper we provide the comparative analysis of three different numerical optimization algorithms and two observability indexes for optimal calibration poses selection.

After we conducted a series of experiments and acquired and pre-processed necessary data, the identification itself can be organised. In most of the related works it is done by linearising forward kinematics relations and then iteratively applying the least-squares algorithm (or its modifications) [2, 6, 8]. While in general this approach should provide better convergence compared to nonlinear optimization, it requires system parametric Jacobian to satisfy certain conditions. In this study we organize search for the original nonlinear problem formulation. The reason for that is described later in the text.

This work is aimed at a comprehensive discussion of experiments and numerical procedures for the open-loop geometric calibration of the KUKA LWR4+ redundant robotic arm, when a full 6D end-effector's pose is measured using Nikon K610 optical CMM. While there are a number of studies reporting successful results on its dynamic identification, we have not been able to identify any work focused on calibration of the robot geometrical parameters. As every external measuring system either a laser tracker or a photogrammetric equipment has it special features and concomitant requirements, an experiment should be adjusted and design of an additional tooling is usually needed. In our case, we designed a special LED fixture and imposed additional constraints for calibration poses selection.

The rest of the paper is organized as follows. In Section 2 we describe the setup and practical issues on organising experiments with the optical CMM. In Section 3 we discuss the problem of selecting optimal calibration configurations and provide comparative analysis of different optimization algorithms and observability indexes followed by its results. In Section 4 we solve the problem of robot's geometric parameters identification. Finally, we conclude the paper with analysis of the obtained results and discussion on future steps.

2. Optimization of the Calibration Configurations

2.1. Problem Statement

An outcome of the geometric calibration is estimations of parameters describing relative location of neighbouring coordinate systems associated with robot links. Basically, it means identifying

parameters of the forward kinematics equation

$$Y^l = F(\Phi, q)|_{q=q^l}\,, \tag{1}$$

where $Y^l = [x^l y^l z^l \phi^l \theta^l \psi^l]^T$ and $q^l = [q_1^l q_2^l \dots q_n^l]^T$ are the end-effector's Cartesian pose and relative to the measurement device and the vector of joint angles for robot's configuration l respectively, n is the number of robot joints, and Φ is the vector of unknown geometric parameters.

It is clear that the calibration is feasible only if a total number of constraint equations (1) from all measurements $l = 1, 2 \dots M$ is bigger than a number of estimated parameters. However, a good selection of the configurations is more important than its number to obtain good identification results.

As a quantitative measure of the configurations optimality, several so-called observability indices $O(Q)$, $Q = \{q^1, q^2 \dots q^M\}$, were introduced (refer to [4, 6] for more details). However, all of these indexes rely on properties of the Jacobian evaluated in $l = 1, 2 \dots M$ configurations

$$J(Q) = \left[J^1; J^2; \dots; J^M\right], \tag{2}$$

where J^l in the Jacobian defined in the configuration q^l

$$J^l = \left.\frac{\partial F(\Phi, q)}{\partial \Phi}\right|_{q=q^l}.$$

Thus, the configurations optimization task can be formulated as a nonlinear constraint optimization problem

$$\max_Q O(Q), \quad \texttt{subject to} \tag{3}$$

$$\begin{cases} q_i^l \in (q_{i,min}; q_{i,max}), \\ Y^l \in (Y_{min}; Y_{max}), \end{cases} \quad \forall i = 1 \dots n,\ l = 1 \dots M \tag{4}$$

The most common way of composing the forward kinematics equation (1) is to use a set of modified Denavit-Hartenberg (mDH) parameters

$$\Phi = [\alpha_0, \dots \alpha_{n+1}, d_0, \dots d_{n+1}, \theta_0, \dots \theta_{n+1}, r_0, \dots r_{n+1}]$$

and a homogeneous transformation

$${}^{j-1}T_j = Rot_{x,\alpha_j} Trans_{x,d_j} Rot_{z,\theta_j} Trans_{z,r_j}.$$

For more detailed explanation, please, refer to [9].

2.2. Observability Indices

In this work we validated two different observation indices [6] . The first on is the inverse condition number of the Jacobian (2)

$$O_1 = \frac{\sigma_{min}}{\sigma_{max}},$$

where σ_{min} and σ_{max} are Jacobian minimal and maximum singular values respectively (see [5]).

The second index was introduced in [2]

$$O_2 = \frac{\sqrt[R]{\sigma_R \dots \cdot \sigma_i \dots \sigma_1}}{\sqrt{M}},$$

where R is the Jacobian rank, M is the number of configurations, and σ_i, $i = 1 \dots R$ are Jacobian singular values.

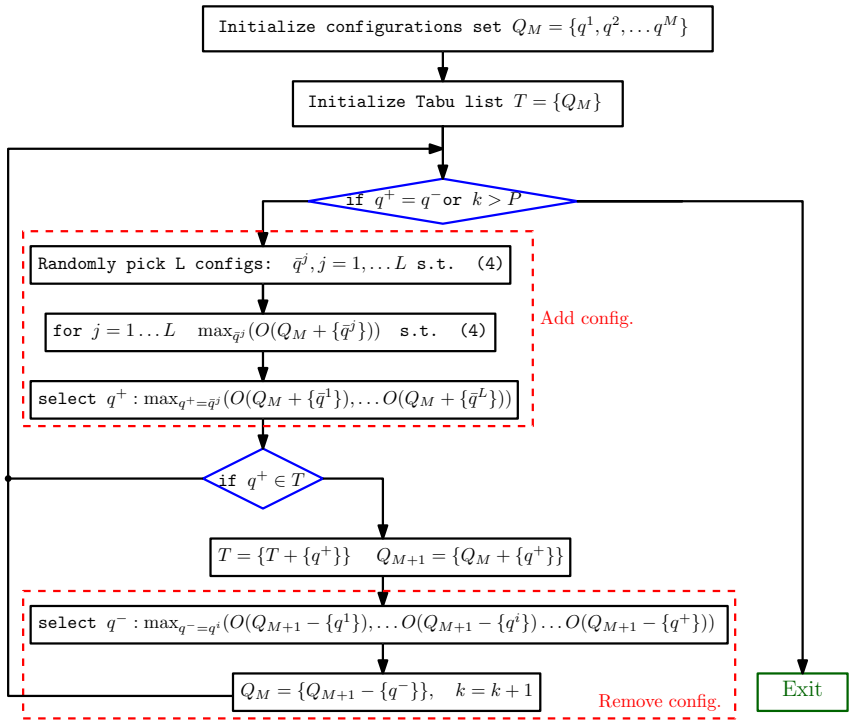

Figure 1: Diagram for the iterative meta-heuristic algorithm algorithm with the Tabu rule

2.3. Eliminating Non-Identifiable Parameters

While a set of mDH parameters is known to be the minimal for robot kinematics representation, depending on a particular calibration setup, some of the parameters in Φ can be non- or poorly identifiable. These parameters are associated with linearly dependent columns of the Jacobian J and consequently with zero of very small Jacobian singular values σ_i.

In order to recursively calculate Jacobian (2) and simultaneously eliminate non-identifiable parameters, we used an approach described in details in [9].

2.4. Pose Optimization Algorithms

We compared performance of three different algorithms for calibration poses optimization.

The first one is conjugate-type deterministic algorithm similar to one described in [9]. It tries to optimize the entire set of configuration on every iteration. However, algorithms of this type have significant limitations: strong dependence on initial conditions and sticking in a local minimum [4].

To avoid these issues we implemented a modification of the previous algorithm utilizing multistart optimization, i.e. when the same algorithm starts N times (we selected $N = 50$) consequently from randomly uniformly distributed initial conditions.

As an alternative to conjugate-type algorithms, we tested an iterative meta-heuristic algorithm with the Tabu rule [4]. Instead of optimizing the entire configurations set, it implements a 2-stage iterative procedure (see Fig. 1). Tabu list T here is a set of already verified configurations, which is introduced to prevent a premature convergence of the algorithm to local minima. This scheme is quite similar to genetic algorithms, while a stochastic behaviour is introduced here by randomly selecting candidate configurations on each *'Add config.'* step.

We selected $L = 10$ and $P = 2M$. Compared to the conjugate-type algorithm, the optimization task takes only n variables instead of $n \times M$, but should be solved $L \times P$ times.

We used a SQP (sequential quadratic programming) solver for all aforementioned algorithms.

3. Identification of the Geometric Parameters

Let us introduce a vector of discrepancies between the predicted and measured end-effector's Cartesian position

$$\Delta Y = Y_m - Y_c, \tag{5}$$

where $Y_m = \left[Y_m^1, Y_m^2 \dots Y_m^M\right]$ is the vector of measured poses and $Y_c = \left[Y_c^1, Y_c^2 \dots Y_c^M\right]$ is the vector of poses calculated from (1).

In the most of classical works forward kinematics relations (1) are linearised using Taylor series expansion such that

$$\Delta Y = J_B \Delta \Phi_B, \tag{6}$$

where the base parametric Jacobian J_B is defined from (2) eliminating linearly dependent columns and $\Delta\Phi_B$ is the vector of base parameters' correction.

In this case parameters estimates $\hat{\Phi}_B$ can be found iteratively applying ordinary least-squares solution or its damped or weighted modifications (for details refer to [6]) that minimizes the performance index $\Delta Y^T \Delta Y$

$$\begin{aligned} \Delta\Phi_{B,k} &= J_B^+ \Delta Y_k, \\ \hat{\Phi}_{B,k} &= \hat{\Phi}_{B,k-1} + \Delta\Phi_{B,k}, \end{aligned} \tag{7}$$

where J_B^+ is the pseudo-inverse of the matrix J_B.

However, convergence of the algorithm (7) is guaranteed only for well-conditioned problems when $O_1 \geq 0.01$ [6]. As we can see from Table 3 we were not able to meet this requirement for the selected setup, even applying different non-identifiable parameters elimination and parameter scaling techniques [2, 6, 8, 9]. Therefore, instead of applying (5)-(7), we formulated the identification task as a nonlinear optimization problem of finding a vector of parameters estimates $\hat{\Phi}$ such that it minimizes the norm of output residual (5)

$$\left|\left| Y_m - F(\hat{\Phi}, Q) \right|\right| \rightarrow \min .$$

4. Experimental Results

4.1. Setup Description

KUKA LWR4+ is a redundant robotic arm with 7 rotational joints. It offers unique features via its low-latency Fast Research Interface (FRI) developed with focus on research purposes [7]. At the same time, to the best of our knowledge, the only source of geometrical parameters' data for this robot is a CAD model, which provides quite rough estimations.

There are different kinds of metrological equipment suitable for calibration experiments, including laser trackers [10] and photogrammetric systems [11], which are considerably less expensive. We use the latter type Nikon K610 system. This optical CMM allows us localizing end-effector in 3D space with sampling rate up to 1kHz and volumetric accuracy of 60 μm for measurement volume of 17 m^3. This way, having complete 6D pose measurements in calibration experiments we are able to identify the maximum number of robot's geometric parameters [6, 8]. Tracking movable objects is enabled through dynamic frames concept [3]. The system defines positions of infrared LEDs by means of three linear CCD cameras scanning in different planes. Diodes on/off phases are synchronized via strobers such that the camera 'distinguish' between different LEDs.

One more element, which is needed for calibration, is a fixture with LEDs that should be attached to a robot tool plate. Based on Nikon specifications, an LED is guaranteed to be visible only if an angle between a normal to its surface and a line of sight with the camera's central point does not exceed 30°. It gives us 'a visibility cone' of each LED. Thereby, a pyramid geometry was optimized based on criteria:

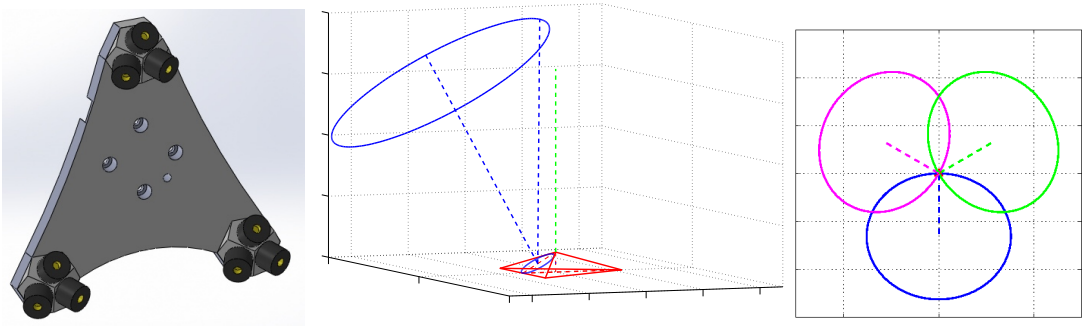

(a) Fixture CAD model (b) Pyramid geometry (c) LEDs' visibility cones: top view

Figure 2: LEDs fixture geometry

Table 1: Nominal mDH parameters

Frame	α_i, [rad]	d_i, [m]	θ_i, [rad]	r_i, [m]
0	0	0	1.549	-4.407
1	1.528	0.067	$q_1 - 0.815$	-0.137
2	$\frac{\pi}{2}$	0	q_2	0
3	$-\frac{\pi}{2}$	0	q_3	0.4
4	$-\frac{\pi}{2}$	0	q_4	0
5	$\frac{\pi}{2}$	0	q_5	0.39
6	$\frac{\pi}{2}$	0	q_6	0
7	$-\frac{\pi}{2}$	0	$q_7 - 0.268$	$2.2 \cdot 10^{-3}$
8	0	0.014	1.0523	0.079

- all three 'visibility cones' have at least one common point on a distance of $1.5m$[1] from the pyramid top, i.e. there is no 'blind spot' in between
- pyramids' sides allows to inscribe a circle about a size of a LED

Geometry behind the calculation is illustrated on Fig. 2b–2c. We have chosen a design with nine LEDs arranged in triples on sides of three similar pyramids, which are distributed on the plate surface (see Fig. 2a).

Fig. 3 illustrates relations between different coordinate frames for the calibration setup.

Nominal mDH parameters values for the considered system are in the Table 1 [2].

Except for physical limitations on joint angles, we should impose additional constraints on the LEDs fixture Cartesian coordinates. Despite the fact that we can place the camera to cover the entire robot workspace, the end-effector pose can be recovered only if at least 3 LEDs remain

[1] The distance of 1.5 m was selected based on the relative location of the camera and the robot and parameters of the camera's field of view.

[2] While the robot parameters ($i = 1 \dots 7$) were taken from the CAD model, parameters of the transformation between the camera and the robot base frames (indexed with z) were calculated backwards from camera-based measurements, and parameters for the transformation between the robot last joint and LEDs fixture frames (indexed with e) were directly measured.In general, the Nikon camera allows direct measurements of the end-effector's pose relative to the robot base, therefore transformation between the camera and the robot base coordinate frames can be excluded from consideration.

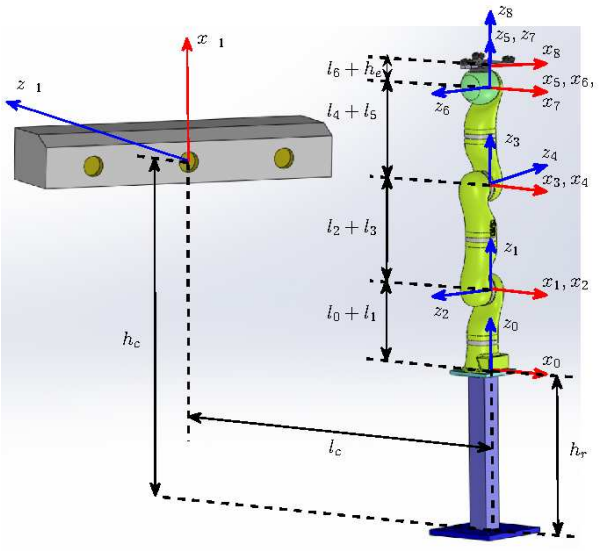

Figure 3: Coordinate frames for camera, robot, and LEDs fixture

Table 2: Constraints for Configurations Optimization

Parameter	**Constraint**
Joint angles, [rad]	$q_{1,3,5,7} \in [-\frac{17\pi}{18}, \frac{17\pi}{18}]$, $q_{2,4} \in [-\frac{2\pi}{3}, \frac{2\pi}{3}]$, $q_6 \in [-\frac{\pi}{2}, \frac{\pi}{2}]$
Fixture roll, [rad]	$\phi_{x,LED} \in [-\frac{4\pi}{9}, \frac{7\pi}{18}]$
Fixture pitch, [rad]	$\theta_{y,LED} \in [-\frac{\pi}{4}, \frac{\pi}{4}]$
Distance between LED TCP and robot base, [m]	$\sqrt{{}^0x_8^2 + {}^0y_8^2} \geq 0.2$
z-coordinate of LED TCP, [m]	${}^0z_8 \geq -0.1$

visible. It gives us bounds on roll, pitch, and yaw angles of the LEDs fixture, expressed in the camera coordinate frame. Two more constraints were imposed to guarantee that the LEDs fixture will not collide with the robot base. All these constraints are summarized in Table 2.

4.2. Identification Results

As initial conditions for the optimization procedure we randomly selected M robot configurations, satisfying (4), such that it was uniformly distributed across the robot's workspace and provided distinguishable variation in joint angles as well.

As the result of the non-identifiable parameters elimination procedure, we determined that 4 parameters θ_0, r_0, θ_8, and r_8 are non-identifiable that defines a set of $4(n+2)-4 = 32$ base parameters Φ_B to be calibrated and the base parametric Jacobian J_B of size $[6M \times 32]$.

Comparative results of the optimization for sets of 10 and 20 configurations for all three algorithms and two observability indices are given in Table 3.

Fig. 4 illustrates how joint angles change between initial and optimized calibration configurations.

Fig. 5 visualizes how robot end-effector positions (relative to the camera coordinate frame) change between nominal and optimized calibration configurations.

Table 3: Optimised Observability Indices

Number of Config.	**Algorithm**	**Observability Index**	
		O_1	O_2
$M = 10$	Non-optimized	0.000716	0.5685
	Conjugate-type deterministic	0.001535	0.8065
	Conjugate-type with multistart	0.001613	0.7955
	Randomized iterative with Tabu rule	0.001497	0.7904
$M = 20$	Non-optimized	0.000811	0.6435
	Conjugate-type deterministic	0.001618	0.8142
	Conjugate-type with multistart	0.001631	0.7973
	Randomized iterative with Tabu rule	0.001571	0.8091

Table 4: Calibrated mDH parameters

Frame	α_i, [rad]	d_i, [m]	θ_i, [rad]	r_i, [m]
0	0.01515	$1.07 \cdot 10^{-2}$	1.549	-4.407
1	1.52662	$2.7 \cdot 10^{-3}$	$q_1 - 0.815$	-0.147
2	1.57093	$-2.5 \cdot 10^{-4}$	$q_2 - 3.9 \cdot 10^{-3}$	$1.3 \cdot 10^{-4}$
3	-1.57029	$-2.5 \cdot 10^{-4}$	$q_3 - 9.7 \cdot 10^{-3}$	0.399
4	-1.57031	$1.0 \cdot 10^{-3}$	$q_4 - 6.5 \cdot 10^{-3}$	$2.5 \cdot 10^{-4}$
5	1.57025	$-9.1 \cdot 10^{-4}$	$q_5 + 8.3 \cdot 10^{-4}$	0.391
6	1.57274	$3.9 \cdot 10^{-4}$	$q_6 - 1.6 \cdot 10^{-3}$	$9.5 \cdot 10^{-5}$
7	-1.57261	$-5.7 \cdot 10^{-4}$	$q_7 - 0.267$	$1.1 \cdot 10^{-2}$
8	$6.5 \cdot 10^{-4}$	$-1.2 \cdot 10^{-4}$	1.053	0.079

And finally, Fig. 6 shows if the constraints imposed on the LEDs fixture position and orientation were matched.

For the calibration experiment we used a set of $M = 20$ optimised configurations found by the conjugate-type algorithm with the observability index O_1. Out of this set we picked $M = 17$ configurations, where we had good visibility of LEDs.

Estimated values for system's mDH parameters are in Table 4.

Fig. 7 illustrates the difference in calculated end-effector's Cartesian positions when nominal and calibrated (identified) parameters sets are used. It is clear that for estimated geometric parameters predicted values are much more closer to the measured ones.

5. Conclusions and Future Work

This work discusses the problem of robot kinematic calibration.

Open-loop geometric calibration of the KUKA LWR4+ redundant robotic arm, when a full 6D end-effector's pose is measured using Nikon K610 optical CMM considered as a particular example. To the best of our knowledge, such an experiment is a unique attempt on its own.

We compared 3 different algorithms and 2 observability indices solving the configurations optimization task. Comparative analysis of the obtained results leads to the following conclusions:

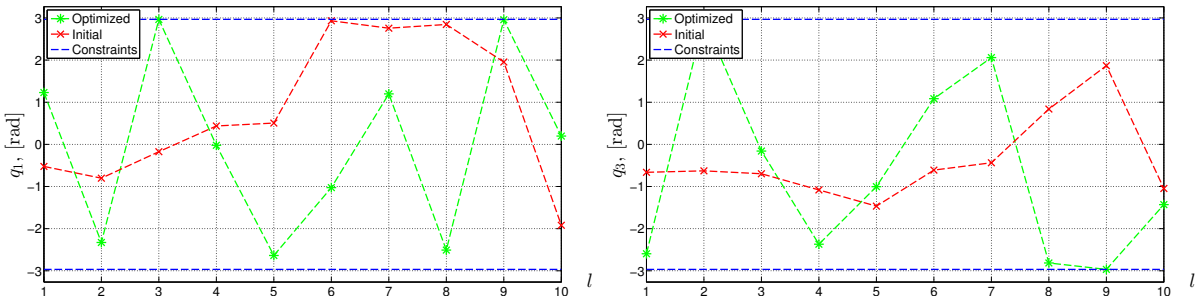

(a) Conjugate-type algorithm, O_1

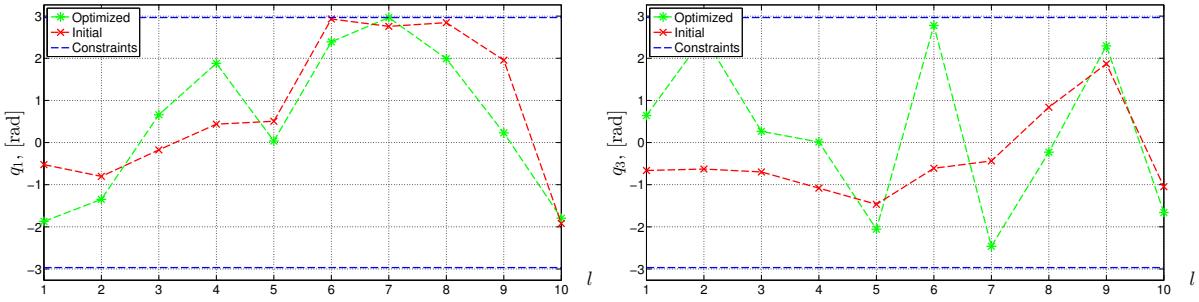

(b) Conjugate-type algorithm, O_2

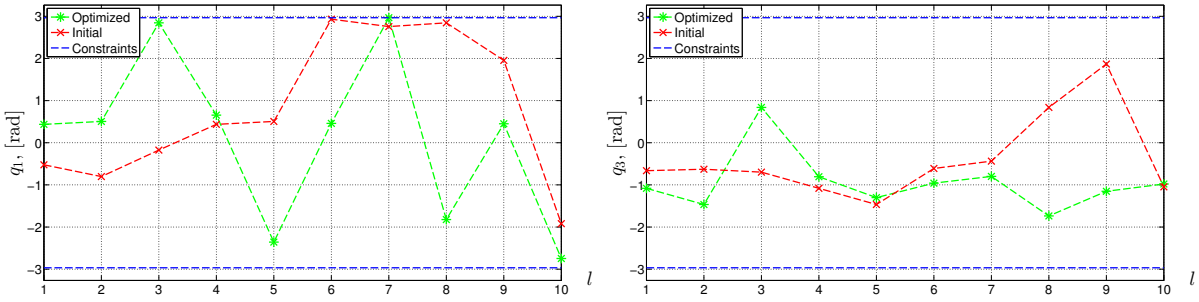

(c) Iterative algorithm, O_1

Figure 4: Joint coordinates for $M = 10$ selected calibration poses (only q_1 and q_3 are presented for illustration purposes)

- Optimization algorithms gave tangible difference in terms of joint configurations and end-effector's poses allocation, but provided quite similar resulting observability indices. It reveals features of the cost function, which is highly nonlinear and has many local minimums.
- The observability index O_1 associated with the Jacobian condition number shows higher relative improvement between initially selected and optimized configurations compared to the Born-Menq index O_2.
- In practice, the iterative meta-heuristic algorithm with Tabu rule didn't ensure better results, while required longer computation time.

Afterwards, based on the experimental data we estimated system's modified DH parameters that define geometric relations between consequent joint frames. Instead of the traditional approach we solved the original nonlinear identification task. Identification results show that there is a difference in range of $[0.001 \dots 0.01]$ [rad] for angular displacements and in range of $[0.3 \dots 3]$ [mm] for linear displacements between nominal parameters provided by robot's manufacturer and its estimated values.

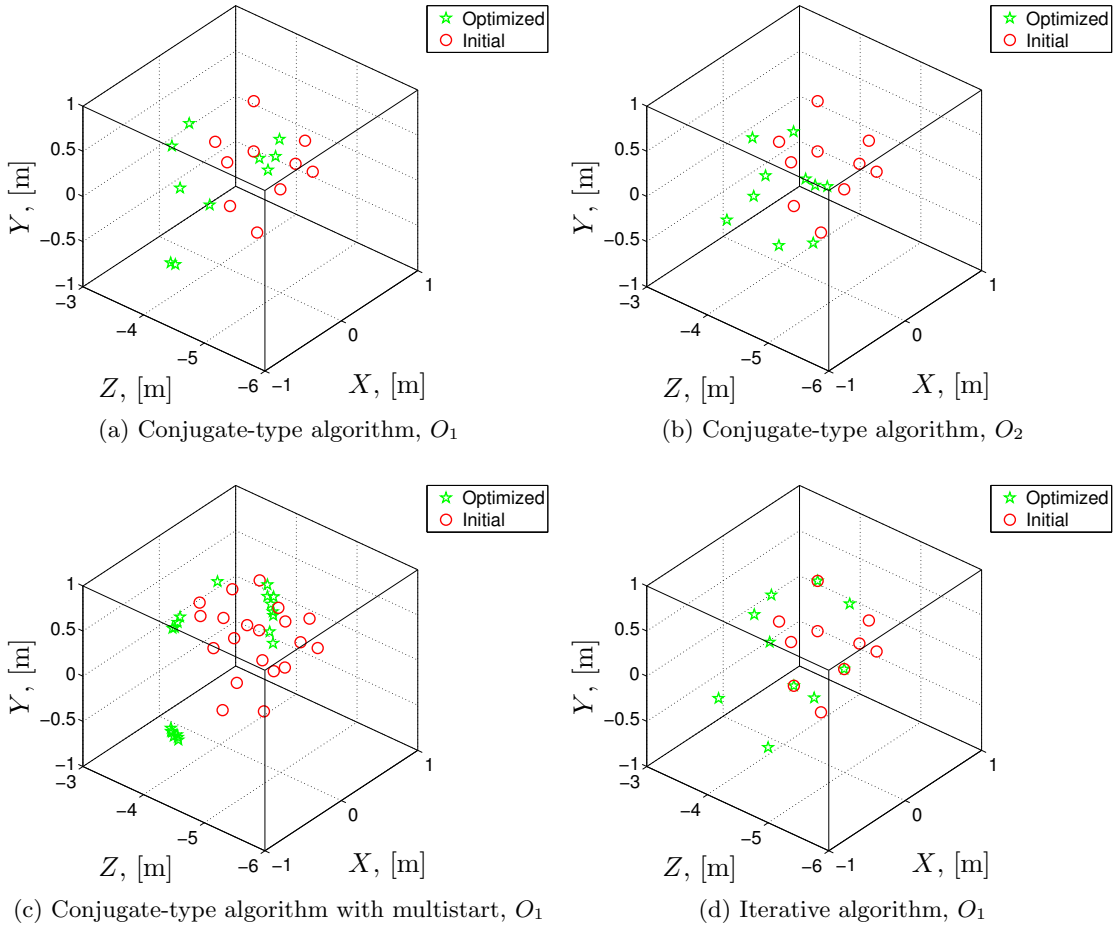

(a) Conjugate-type algorithm, O_1

(b) Conjugate-type algorithm, O_2

(c) Conjugate-type algorithm with multistart, O_1

(d) Iterative algorithm, O_1

Figure 5: LED frame Cartesian coordinates for $M = 10$ selected calibration poses

The proposed procedure is highly automated and can be implemented to improve manipulator's performance both right after the installation for initial calibration and on a periodic basis, since estimated parameters can deviate because of the tear and wear and other factors.

References

[1] ISO 9283:1998, *Manipulating industrial robots Performance criteria and related test methods.*
[2] Borm J H and Menq C H 1991 Determination of optimal measurement configurations for robot calibration based on observability measure, *J. of Robotic Systems* **10** 51-63
[3] van den Bossche A 2004 Procedure for determining the dynamic behavior of a vehicle on a test bench *US Patent 6,748,796*
[4] Daney D, Y. Papegay Y and Madeline B 2005 Choosing measurement poses for robot calibration with the local convergence method and Tabu search *The Int. J. of Robotics Research* **24** 501-18
[5] Driels M R and Pathre U S 1990 Significance of observation strategy on the design of robot calibration experiments *J. Robot. Sys.* **7** 197-223
[6] Hollerbach J M and Wampler C 1996 The calibration index and taxonomy for robot kinematic calibration methods *Int. J. Rob. Res.* **15(6)** 573-91
[7] Schreiber G, Stemmer A and Bischoff R 2010 The Fast Research Interface for the KUKA Lightweight Robot *Proc. IEEE ICRA 2010 Workshop on Innovative Robot Control Architectures*
[8] Khalil W, Besnard S and Lemoine P 2000 Comparison study of the geometric parameters calibration methods *Int. J. of Robotics and Automation* **15(2)** 56-67

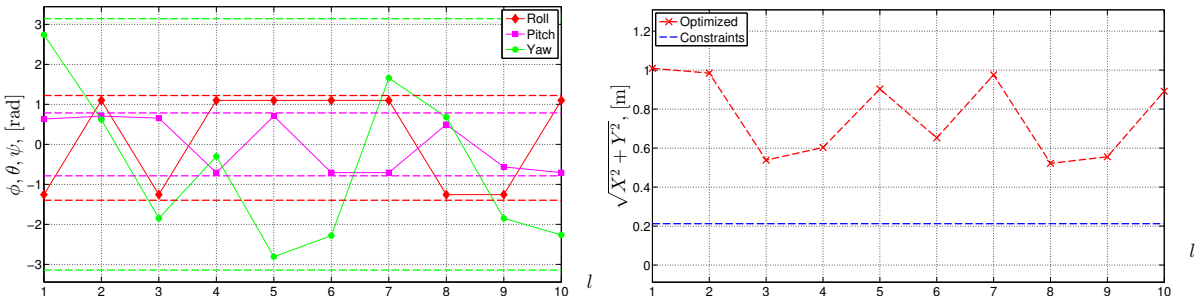

(a) Conjugate-type algorithm, O_1

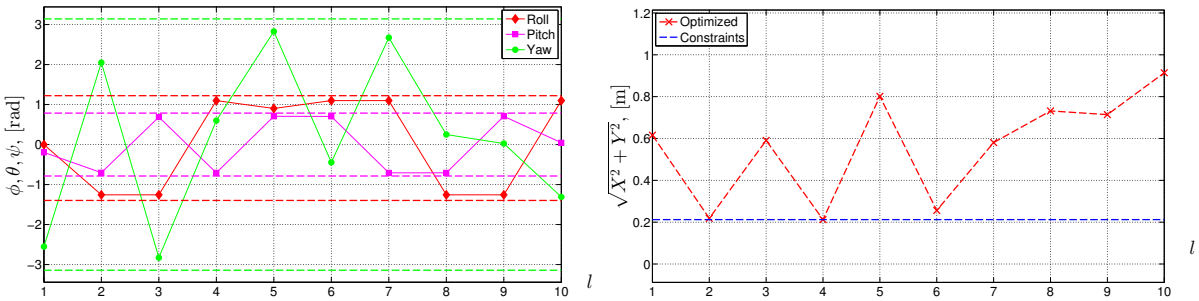

(b) Conjugate-type algorithm, O_2

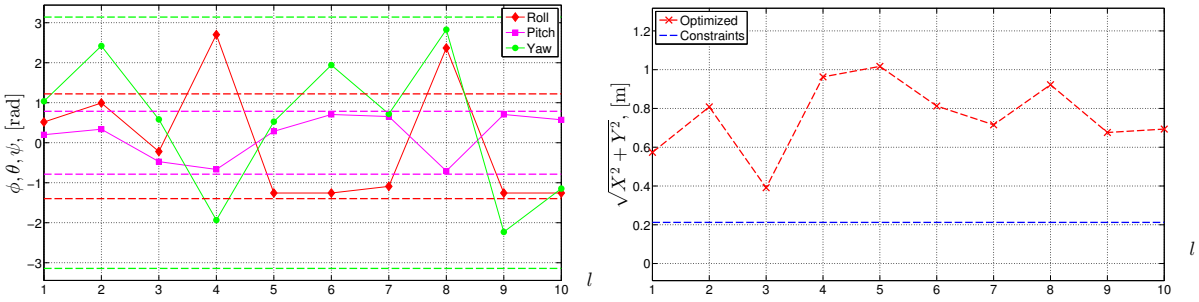

(c) Iterative algorithm, O_1

Figure 6: Constraints for the LED frame orientation and its distance from the robot base for $M = 10$ selected calibration poses

[9] Khalil W, Gautier M and Enguehard Ch 1991 dentifiable parameters and optimum configurations for robots calibration *Robotica* **9** 63-70

[10] Klimchik A, Pashkevich A, Wu Y, Caro S and Furet B 2012 Design of calibration experiments for identification of manipulator elastostatic parameters *J. of Mechanics Engineering and Automation* **2** 531-42

[11] Marie S, Courteille E and Maurine P 2013 Elasto-geometrical modeling and calibration of robot manipulators: Application to machining and forming applications *Mechanism and Machine Theory* **69** 13-43

[12] Renders J M, Rossignol E, Becquet M and Hanus R 1991 Kinematic calibration and geometrical parameter identification for robots *IEEE Transactions on Robotics and Automation* **7(6)** 721-32

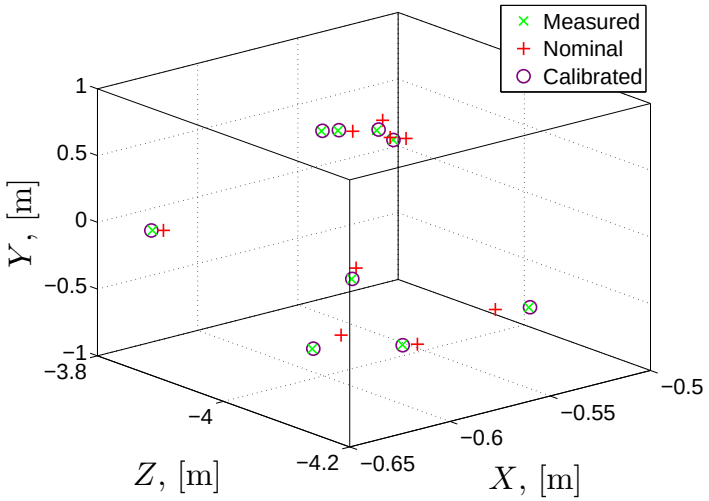

(a) 3D pose, zoomed area

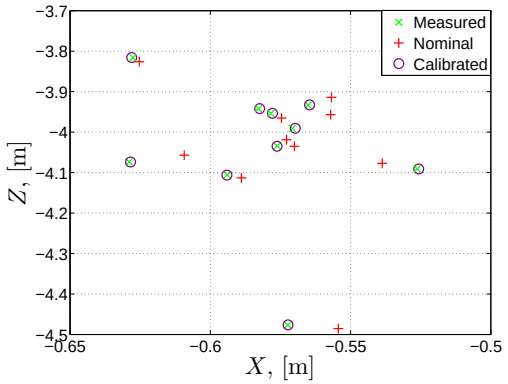

(b) Projection on the XZ plane, zoomed area

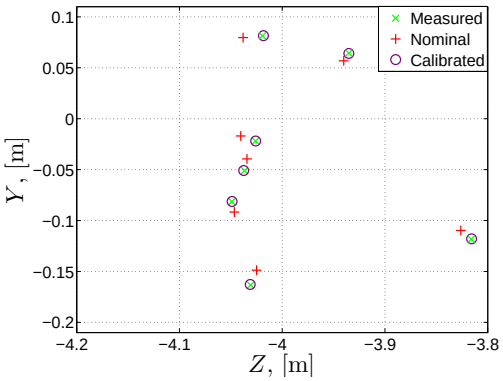

(c) Projection on the YZ plane, zoomed area

Figure 7: Comparison of end-effector's Cartesian coordinates for nominal and calibrated geometric parameters